Acta Geodyn. Geomater., Vol. 23, No. 2 (222), 263–278, 2026
DOI: 10.13168/AGG.2026.0017
journal homepage: https://www.irsm.cas.cz/acta

ORIGINAL PAPER

THREE-DIMENSIONAL UNIAXIAL DISCRETE ELEMENT SIMULATION AND MESOSCOPIC ANALYSIS OF THERMAL DAMAGE AT HIGH TEMPERATURE IN SANDSTONE

Guang Chuan LIANG [1], Qi Hua ZHAO [1,*], Bo WANG [1], Lu LU [2] and Shuai WANG [2]

[1] *State Key Laboratory of Geohazard Prevention and Geoenvironment Protection, Chengdu University of Technology, Chengdu, Sichuan, 610059, China*
[2] *CCCC Highway Consultants Co., Ltd, Chengdu, Sichuan, 610000, China*

**Corresponding author's e-mail:* zhaoqj1225@163.com

ARTICLE INFO

Article history:
Received 19 March 2026
Accepted 18 May 2026
Available online 28 May 2026

Keywords:
Sandstone
Thermal damage at high temperature
Micro-scale evolution
Crack network
Mechanical response

ABSTRACT

In view of the severe thermal hazards induced by high temperatures in deep underground engineering, a thermo-mechanical coupling model based on PFC3D is adopted to investigate the microstructural evolution and mechanical characteristics of sandstone subjected to high-temperature thermal damage. The results show that: (1) The expansion of thermally induced cracks has a threshold effect and heterogeneous characteristic. The cracking degree increased sharply in the temperature range of 800 °C-1000 °C. Thermally induced cracks presented a central concentration phenomenon and gradually weakened from the core region to both ends of the rock specimen; (2) The incubation stage of thermal damage was mainly dominated by local shear slip. As the temperature increased, thermal deformation triggered the widespread initiation of tensile fractures, leading to a transition of the failure mode to tensile-shear joint yield; (3) The crack network has undergone an evolutionary process from locally preferred orientation to overall randomness distribution. The comprehensive uniformity index indicates that thermal stress will drive the failure behavior of rock, prompting a transition from anisotropy to uniform disintegration; (4) Based on the three-dimensional contact microstructure diagram, it was found that heating below 400 °C would promote the polarization of the force chain. Local strengthening would lead to a slight increase in uniaxial compressive strength, and the thermal damage variable value was relatively low. However, after exceeding 600 °C, the main skeleton collapsed, causing the thermal damage variable approaching 0.8.

1. INTRODUCTION

Due to the surge in global energy demand and the gradual depletion of shallow reserves, the exploitation of geo-resources inevitably shifts to deep-seated underground environments (Wu et al., 2019; Wu et al., 2024). However, the intricate geological environment in deep sea poses a huge challenge to the safe exploitation of these resources. In stark contrast to shallow formations, the characteristics of deep rock masses are controlled by extreme "three-high" mechanisms: increased geothermal temperatures, enormous geo-stress, and high-pore water pressure (Guo et al., 2023). Under the geothermal gradient, the ambient thermal field continuously upgrades with increasing burial depth, often immersing deep geo-mechanical systems in high-temperature environments of hundreds of degrees Celsius (Ranjith et al., 2017). Under strong thermal exposure, the basic crystals and cementation network of rocks were severely damaged, leading to substantial degradation of physical and deformational properties (Showkati et al., 2021). Therefore, the mechanical responses and multi-scale damage mechanisms of rock media under extreme thermodynamic conditions have become a hotspot in geotechnical mechanics and disaster prevention and mitigation (Vidana Pathiranagei and Gratchev, 2021; Tomás et al., 2025). Research on the thermo-mechanical behavior of rocks mainly advances along four different trajectories: capturing transient deformation processes (Wang et al., 2024), establishing temperature-dependent failure criteria (Hu et al., 2023), revealing micro-scale thermal damage mechanisms (Chen et al., 2019), and developing predictive constitutive models (Feng et al., 2020).

Deep surrounding rock masses, represented by quartz-rich silicate rocks including sandstone and granite, are usually exposed to continuous high-temperature thermal shocks exceeding 1000 ℃ in practical engineering. Such extreme internal temperature gradient and thermal cycling will directly lead to irreversible and irreversible deterioration in the physical and mechanical properties of rocks (Ram et al., 2025). Numerous laboratory investigations have verified that the uniaxial compressive strength (UCS), dynamic elastic modulus, and P-wave velocity of rocks often pronounced nonlinear degradation under thermal conditions (Garrido et al., 2022; Liu et al.,

Cite this article as: Liang GC, Zhao QH, Wang B, Lu L, Wang S: Three-dimensional uniaxial discrete element simulation and mesoscopic analysis of thermal damage at high temperature in sandstone. Acta Geodyn. Geomater., 23, No. 2 (222), 263–278, 2026. DOI: 10.13168/AGG.2026.00017

2025). This decrease in macroscopic mechanical bearing capacity is mainly attributed to the complex evolution of internal microstructure of rocks and the irreversible accumulation of thermal damage microcracks (Alneasan et al., 2024). From the perspective of microscopic thermodynamic mechanisms, rocks are essentially heterogeneous bodies composed of multiple minerals. Rock-forming minerals (such as quartz, feldspar and mica) exhibit significant anisotropy and mismatch characteristics in thermal expansion coefficient, thermal conductivity, and thermodynamic phase transition threshold (Yin et al., 2024). When the external thermal load increases and exceeds the temperature threshold (such as the quartz α-β phase transition), highly concentrated and uneven thermal stresses will be generated at the boundaries of adjacent mineral particles and within the crystal nuclei. Once the local thermal stress exceeds the tensile and shear strength of intergranular cementation or mineral crystals, the initiation, intersection, and connection of large-scale intergranular and intragranular cracks will be triggered (Dang et al., 2025). To accurately simulate the micro-fracture process of rocks in the spatial-temporal dimension, the non-destructive acoustic emission (AE) monitoring technology has been adopted to analyze high-temperature damage rocks. The vibration count, three-dimensional spatial positioning, energy release characteristics, and wave patterns of acoustic emission events can directly reflect the entire process of the rock mass, including crack compaction, linear elastic energy storage, and the stable and unstable expansion of microcracks. Meanwhile, these indicators further clarify the fracture dynamics mechanism underlying the transition of rock failure from brittle splitting to ductile or quasi-plastic shear yielding under high-temperatures (Griffiths et al., 2024; Harshini et al., 2024). However, only relying on traditional physical mechanics experiments and acoustic emission monitoring techniques remains insufficient to achieve full-scale, high-resolution quantitative characterization of the heterogeneous expansion paths and force chain evolution in 3D rock fracture network.

With the rapid advancement of computational rock mechanics, numerical approaches based on the discrete element method (DEM) and finite element method (FEM) have emerged as effective digital tools for investigating thermally induced damage in rock materials (Rezaee and Noorian-Bidgoli, 2025). In the finite element method, Bao et al. (2025) used ABAQUS to investigate the failures of high-temperature rocks under uniaxial cyclic loading. By quantifying the volume fraction of fracture units, they clarified the intrinsic relationship between the Kaiser effect and cumulative damage. Yoo et al. (2023) focused on the main rock of high-level radioactive waste (HLW) disposal facilities and used the TOUGH-FLAC continuum simulator to decode thermal water mechanical (THM) interactions. Subsequent sensitivity analysis showed that parameters such as thermal conductivity, thermal expansion, Young's modulus, and permeability have measurable effects on multi field response, emphasizing the importance of precise macroscopic calibration. In addition, Günindi et al. (2024) used ANSYS Fluent to simulate thermal fluid interactions, evaluate the high-temperature thermal storage characteristics of basalt glass, quantify its strong energy retention ability, and establish this basalt as a highly feasible alternative medium for extreme temperature applications. Although the finite element method (FEM) performs well in characterizing macroscopic thermal fields, it is limited in discontinuous fracture kinematics due to predefined yield criteria. In contrast, the discrete element method (DEM) can clearly simulate particle interactions and bond breakage, with significant advantages in simulating the spontaneous crack propagation, contact changes, and energy dissipation (Sharafisafa et al., 2023; Sun et al., 2024; Pham et al., 2024). For example, Zhu et al. (2025) studied the thermal damage of heterogeneous granite under complex high-temperature and high-pressure conditions using a two-dimensional discrete element model with clear crystal interfaces. They quantified the expansion law of stress-dependent thermal defects and analyzed the transformation mechanism between tensile fracture and shear yield. Under the background of thermal cooling, Huang et al. (2016) studied the interaction and propagation of multiple thermal defects using two-dimensional numerical simulation techniques. These planar simulations demonstrate that early thermal fracture formed a quasi-layered array parallel to the temperature gradient, with propagation speeds scaled to $\sim t^{1/2}$, and subsequently degraded into highly curled and clustered crack geometries under severe thermal strain. In addition, Yin et al. (2025) studied the fracture toughness of crystalline rocks under cyclic thermal loading using a grain-based model (GBM). Research has shown that as the temperature and cycle frequency increased, the roughness of the fracture surface of the sample increased and the toughness decreased.

Although extensive research has clarified the mechanical degradation laws of thermally damaged rocks through DEM simulations, it still lacks sufficient investigation to characterize the three-dimensional contact structure analysis of high-temperature rock masses, the heterogeneous development of fractures, and attenuation of uniaxial bearing capacity. To this end, a 3D thermo-mechanical coupling model based on Discrete Element Software (PFC3D) is proposed to analyze the mesoscopic damage evolution and progressive failure laws of sandstone at high-temperature conditions. Then a comprehensive uniformity index (S) is introduced to quantitatively analyze the spatial-temporal evolution of thermal damage from local preferred orientation to disordered disintegration. By analyzing the collapse characteristics of the main force transmission skeleton, the mesoscopic mechanism of the sharp drop

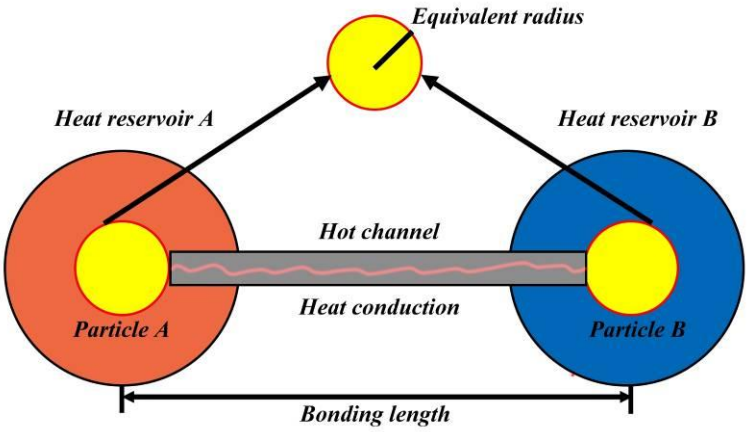

Fig. 1 Heat Conduction Mode.

Table 1 Microscopic parameters of thermophysics.

Microscopic parameters	Symbol	Value
Coefficient of thermal expansion/K^{-1}	A	2.5×10^{-4}
Thermal resistance/$K\cdot(W\cdot m)^{-1}$	H	0.5
Specific heat capacity/$J\cdot(kg\cdot K)^{-1}$	C_v	800

in the compressive strength of sandstone is clarified. The findings will provide a support for safe operation and disaster control of deep underground engineering in high-temperature environments.

2. PFC THERMAL COUPLING THEORY AND THREE-DIMENSIONAL UNIAXIAL SIMULATION PROCESS

2.1. INTRODUCTION TO THE THERMAL MODEL

Based on the PFC discrete element framework, thermal energy transport relies on a thermal storage network system constructed within the granular medium. This network takes particle pairs connected by thermal conduction channels as its fundamental unit. When the thermal pipeline is in an activated state, it assumes the function of heat transportation. The heat conduction behavior strictly follows Fourier's law (Wanne and Young, 2008) (Fig. 1), and the energy transfer is as expressed as follows:

$$Q = -\frac{\Delta T}{\eta L} \tag{1}$$

where Q represents the fixed energy, W; η is the thermal resistance, K/(W·m); L is the interface bonding length, m; ΔT represents the temperature difference at both ends of thermal transfer channel, K.

In the theoretical model established for a single reservoir particle, the heat transfer process within it can be described as follows:

$$-\sum_{p=1}^{N} Q_p + Q_v = \rho C_v \frac{\partial T}{\partial t} \tag{2}$$

where p represents the thermal channel connecting the reservoir units; N is the total number of thermal channels; Q_v represents the heat source density, W/m^3; ρ is the medium density, kg/m^3; C_v is the specific heat capacity, J/(kg·K), and t is the heat conduction, s.

The PFC model is capable of characterizing transient heat conduction processes and capturing thermally induced strain and stress evolution under variable temperature conditions. The particle size is dynamically adjusted based on the coefficients of thermal expansion and temperature distribution, thereby increasing the linear contact force (Eq. (3)). If a linear parallel bonding model is used for particle contact, it can be assumed that the temperature changes will affect the normal contact force $(\Delta\bar{F})$ of the parallel bond, thereby achieving the thermo-mechanical coupled expansion response. In addition, assuming that the thermal expansion properties of parallel bonding are isotropic. The length of parallel bond changes with temperature, thereby changing the contact force, expressed as follows:

$$\Delta R = \alpha R \Delta T \tag{3}$$

$$\Delta\bar{F} = -\bar{K}_n A \Delta U_n = -\bar{K}_n A(\bar{\alpha}\bar{L}\Delta T) \tag{4}$$

where ΔR is particle radius change, m; α is the coefficient of linear thermal expansion, K^{-1}; R is original radius of particles, m; ΔT represents the temperature change, K; $\bar{K}_n$ is the normal stiffness of parallel bonds, N/m; A is the cross-sectional area (CSA) of parallel bonding contact, m^2; $\bar{\alpha}$ is the coefficient of linear thermal expansion of the parallel bonding material (defaulting is the average value of particle coefficients at both ends of the thermal channel), K^{-1}.

Unlike the finite element method based on continuum and the two-dimensional discrete element method, this three-dimensional thermal model explicitly combines the asynchronous thermal expansion of non-uniform grains with the real-time degradation of a three-dimensional parallel bonding

Table 2 Microscopic Parameters of the Linear Parallel Bond Model.

Microscopic parameters	Symbol	Values
Minimum particle radius(mm)	R_{min}	1.0
Maximum particle radius(mm)	R_{max}	1.66
Porosity	n	0.16
Density (kg/m³)	ρ	2500
Particle contact modulus (GPa)	E	10.0
Particle stiffness ratio	k	1.5
Parallel bond modulus (GPa)	$\bar{E}$	10.0
Normal to shear stiffness ratio of parallel bond	$\bar{k}$	1.5
Tensile strength of parallel bond (MPa)	t	29.35
Cohesion strength of parallel bond (MPa)	c	19.57
Friction angle of parallel bond (°)	φ	30
Coefficient of particle friction	μ	0.5

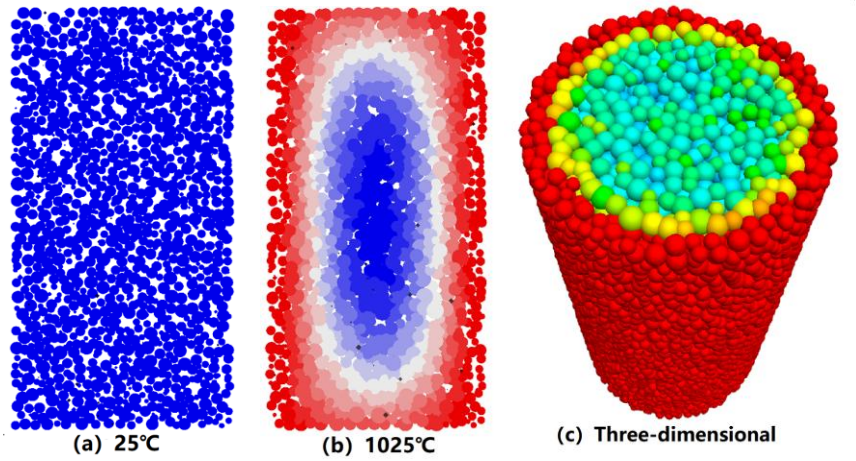

Fig. 2 The external temperature gradually spreads to the interior of rock sample.

network. This micro mechanical mapping enables microcracks to spontaneously initiate and merge without pre-defined fracture paths, directly simulating the structural collapse of the main load-bearing skeleton. Thermal physical parameters mainly include the coefficient of thermal expansion, which affects the expansion and stress increase of particles during heating. Thermal resistance is related to the rate of heat conduction and the specific heat capacity, as shown in Table 1.

In reality, the thermal expansion coefficient and specific heat capacity of sandstone are temperature-dependent and exhibit nonlinear growth at high temperatures. However, to isolate the mechanical degradation caused by thermal mismatch and maintain computational efficiency, constant representative values were adopted in this model as a conservative simplification. This assumption may slightly affect the transient accumulation rate of local thermal stress. It will not fundamentally change the macro-mechanical failure thresholds or the overall evolution mode of the fracture network.

2.2. SIMULATION PROCESS OF THERMAL DAMAGE AT HIGH TEMPERATURE

The rock samples were sandstone, with a corresponding uniaxial compressive strength of 111.2 MPa and elastic modulus of 24.6 GPa. The contact between particles is modeled using a linear parallel bond model to better simulate the mechanical behavior of rocks. The widely accepted "trial-and-error method" is sued to repeatedly calibrate the microscopic parameters. The microstructural parameters of the Linear Parallel Bond Model are shown in Table 2. First, a standard cylindrical sample with a diameter of 50 mm and a height of 100 mm was used to study the deformation, failure and strength of rock samples under indoor conditions at 25 ℃ (298.15 K). It was used as the basic reference sample P0. Then, the external temperature was raised to 225, 425, 625, 825 and 1025 ℃ (the sample numbers were P200, P400, P600, P800 and P1000, respectively), and the external temperature was constant. The time step was controlled at 4×10^{-8} and the cycle was 10000 steps. After that, the external temperature was revoked and another cycle of 200 steps was conducted. The temperature gradually spreads from the outside to the inside, as shown in Figure 2. At the heating stage, the lateral surface of the cylindrical specimen remains

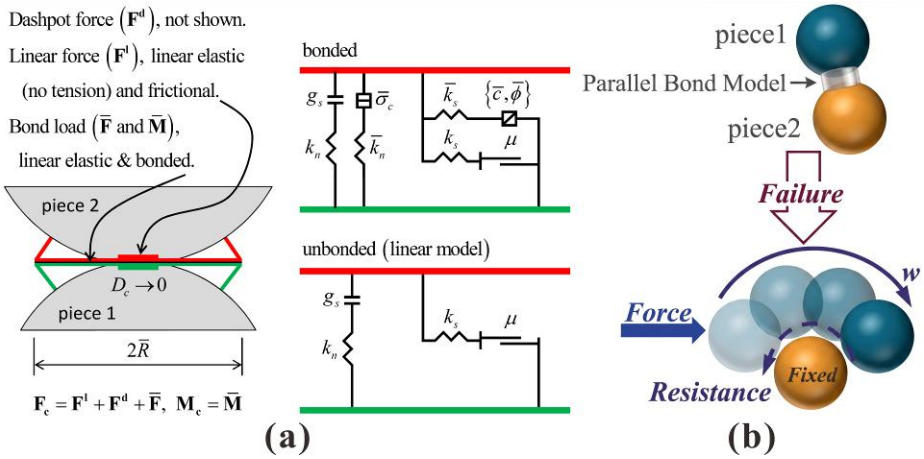

Fig. 3 Mechanical behavior of the linear parallel bond model: (a) Schematic diagram of the parallel bond model; (b) Rotation process of the particles after failure.

unconstrained, and its axial displacement is restricted. Finally, a uniaxial compression test was conducted to study the fracture evolution and strength of sandstone under high temperature.

To precisely simulate the cementation mechanism between sandstone particles, the linear parallel bond model is adopted. As shown in Figure 3(a), this parallel bond model superimposes a finite-sized elastic cementing material onto a basic linear contact framework, enabling simultaneous transmission of interface forces and moments (Potyondy, 2015). When the maximum tensile or shear stress generated by external loading exceeds the inherent strength of the parallel bond (the tensile strength is related to the microstructural parameter *t*, the shear strength is controlled by the Mohr-Coulomb friction strength and determined by the parameters *c* and φ), microscopic cracks will be triggered. Corresponding tensile or shear cracks are generated. These stress components are calculated based on the continuous variables of the cementing cross-section:

$$\bar{\sigma}_{max} = \frac{\bar{F}_n}{\bar{A}} + \bar{\beta}\frac{\|\bar{M}_n\|R}{\bar{I}} \tag{5}$$

$$\bar{\tau}_{max} = \frac{\bar{F}_s}{\bar{A}} + \bar{\beta}\frac{\|\bar{M}_t\|R}{\bar{J}} \tag{6}$$

where $\bar{F}_n$ and $\bar{F}_s$ represent the normal and shear forces; $\bar{M}_n$ and $\bar{M}_t$ represent the normal (bending) and tangential (twisting) moments; $\bar{A}$ is the cross-sectional area; $\bar{I}$ and $\bar{J}$ are the moment of inertia and polar moment of inertia of the parallel bond's cross-section; R is the bonding radius; and β is the moment contribution factor. When the bond is broken, the cohesive connection is permanently eliminated, causing the local contact kinematics to degenerate into a basic linear frictional model (where the liberated particles undergo independent sliding and rolling governed by the particle friction coefficient μ, as shown in Figure 3(b)). When the tangential force of the particles is greater than the frictional force, rotation will occur:

$$|\bar{F}s| > \mu|\bar{F}n| \tag{7}$$

2.3. *DEFORMATION AND FAILURE LAWS OF THE P0 SAMPLE (AT ROOM TEMPERATURE, WITHOUT THERMAL DAMAGE AT HIGH TEMPERATURE)*

Sandstone showed a progressive failure during uniaxial compression. The initiation and propagation of internal microcracks lead to continuous acoustic emission (AE) activities. Therefore, monitoring the development of cracks can help identify the evolution pattern of acoustic emission. Through the comprehensive evolution curve shown as in Figure 4, the stress-strain path during uniaxial compression, the frequency and cumulative number of AE events can be intuitively reflected. As shown in Figure 4, the mechanical response curve of sandstone under uniaxial compression shows distinct stage characteristics. It can be divided into four stages: (1) Initial compaction stage (OA): under axial loading, the pores of rock sample are compressed, and the compaction effect makes the contact between particles tighter. This curve shows a concave nonlinear growth. There were no AE events. This indicates the sandstone only undergoes recoverable elastic deformation and no irreversible plastic damage; (2) Elastic stage (AB): The internal defects have achieved sliding contact through compaction, and new fractures have not appeared. Therefore, this curve shows an approximate linear relationship, and the elastic modulus tends to stabilize. The acoustic emission activity is weak, and the AE events almost coincide with the axis *y*=0; (3) Plastic yielding stage (BC): As the deviatoric stress increases, the sandstone begins to undergo plastic deformation. The internal cracks are stimulated to develop and expand, resulting in a decrease in resisting deformation of the sample. In view of the macroscopic mechanism, the axial strain rate is higher than the stress loading rate. This causes the stress-strain curve to become convex upward and the elastic modulus to gradually decrease from steep. The number of AE and cumulative AE events begin to increase sharply, indicating a non-steady-state acceleration process of sample failure. At this time, the microscopic cracks gradually advance to the center of the sample. The

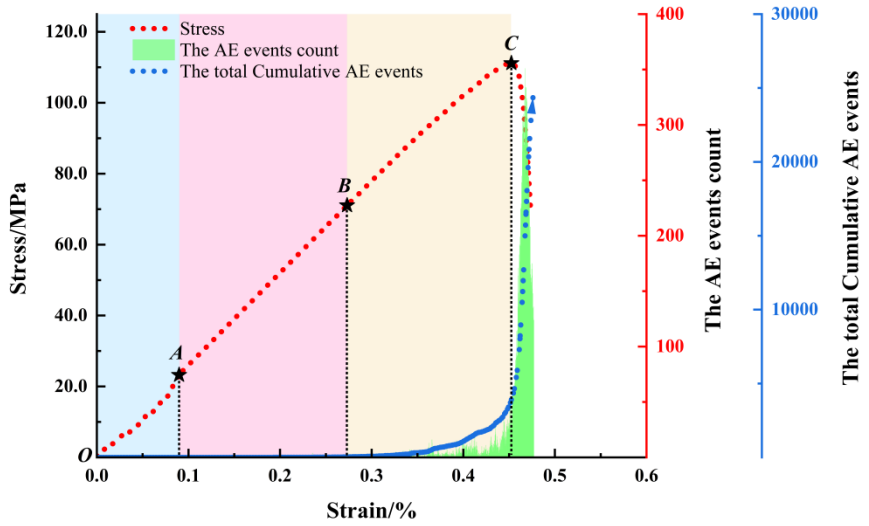

Fig. 4 Stress-strain curve, AE events and the total cumulative AE of sample P0.

rapid increase in AE before the peak strength confirms that although the sample still has a certain load-bearing capacity, serious damage has accumulated internally and is in a critical state close to macroscopic failure; (4) Post-peak failure stage (after point C): After passing through the peak point of stress, this curve shows a strain softening characteristic. The internal fractures of the sandstone continue to develop and converge deeply, ultimately causing the overall failure of the sample. At the same time, the activity of AE signal increases rapidly, and the growth slope of AE accumulation significantly increases, reflecting the intense evolution process of the rock mass from local micro-damage to macroscopic fracture surfaces. Although the stress (bearing capacity) is decreasing, the internal physical damage is accelerating. In the pre-peak stage, the cracks inside the sandstone are mostly isolated and diffusely distributed micro-cracks. Once the peak stress is exceeded, the originally isolated cracks begin to rapidly connect to form a penetrating fracture surface. This large-scale fracture and mutual friction will release more dense and higher-energy sound waves than that in the pre-peak stage, thereby increasing AE events. Based on the monitoring data in Figure 4, the crack initiation stress and peak strength of sandstone can be calibrated, with values of 23.23 MPa and 111.2 MPa respectively. The corresponding strains are 0.09 % and 0.45 %, respectively.

3. RESULT ANALYSIS

3.1. DEVELOPMENT AND EVOLUTION PROCESS OF CRACKS

The density of fracture evolution of sandstone under extremely high-temperature is shown in Figure 5. It has a clear temperature threshold effect and nonlinear expansion characteristic. When the temperature was below 600 °C, there was no significant fracture initiation inside the sample, and the overall framework remained relatively intact. Therefore, only images of high-temperature at 600, 800, and 1000 °C high-temperature heating are listed. However, when the heating temperature reaches the critical threshold of 600 °C (Figs. 5(a) and (d)), the thermal fracture is officially triggered, marking the entry of the rock sample into the damage initiation stage. At this point, the three-dimensional fracture density and its planar sections clearly show that the heat-induced fractures have extremely strong spatial locality and non-uniformity. They are mainly scattered in isolated clusters within the rock mass and have not yet formed effective spatial connectivity. They are mainly distributed at the outer circle of the sample. This indicates that the damage caused by high-temperature is gradually expanding from the outside to the inside. This is mainly attributed to the accumulation of the non-uniform thermal stress field of the sample when the temperature increases, and local thermal stress has overcome the bonding strength of particles. As the heating temperature further increased to 800 °C (Figs. 5(b) and (e)) internal fractures underwent a period of intense expansion and connection. Unlike the isolated distribution at 600 °C, fractures at this temperature showed an explosive growth and developed into a complex three-dimensional connected network in space. It is notable that the spatial distribution of the normalized fracture density showed a significant gradient feature. The high-density damaged areas (the yellow area approaching 1.0) clustered in the center of the sample and showed a decaying trend to both ends of the sample. This typical "central concentration" effect is usually attributed to the asynchrony of heat conduction within the rock at extremely high-temperatures and the superposition of thermal stress gradients. It dominates the evolution path of the macroscopic fracture network. After the sample was heated to 1000 °C (Figs. 5(c) and (f)), thermodynamic

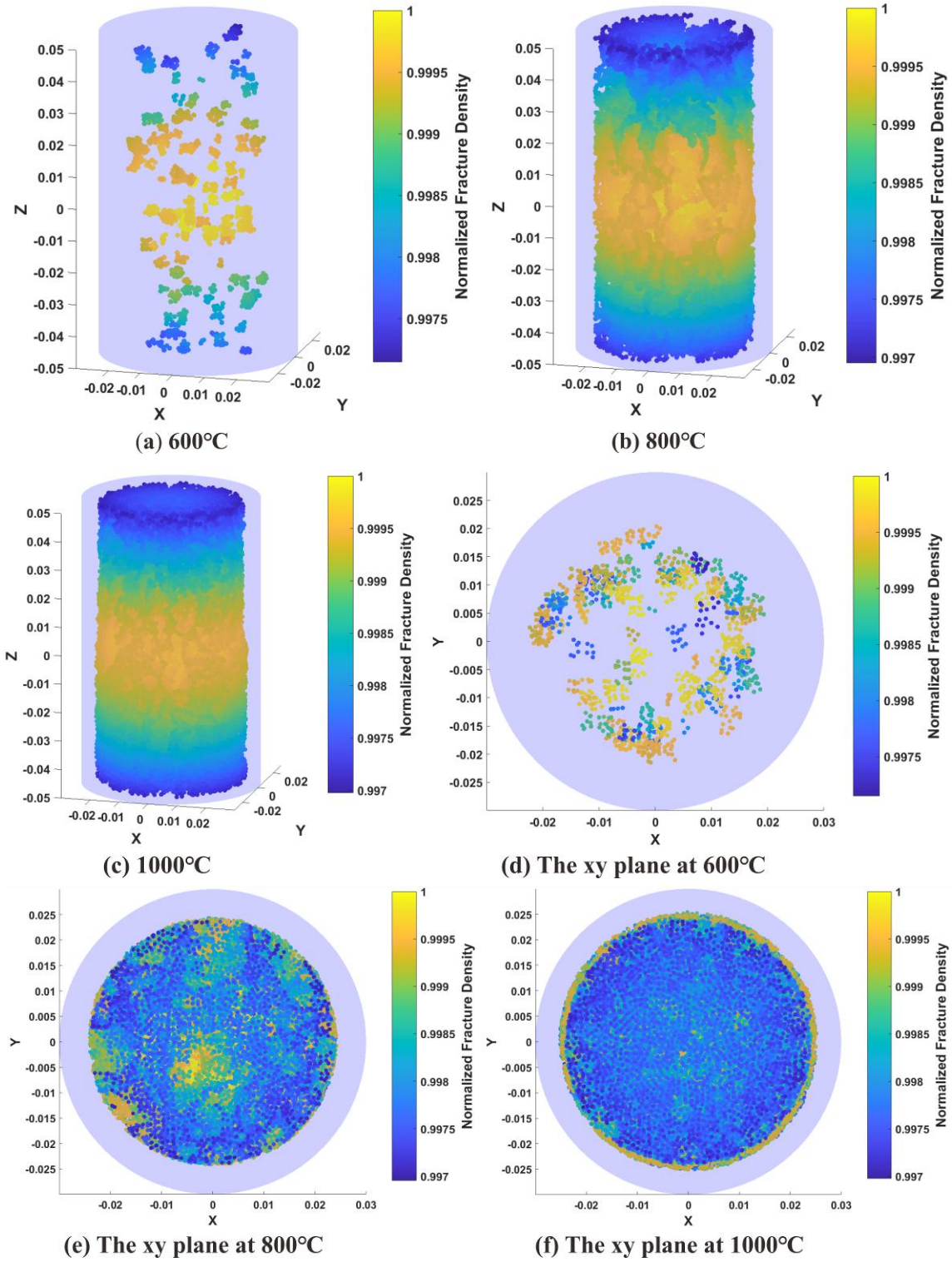

Fig. 5 Fracture density under different thermal damage at high temperatures.

damage of the rock reached an almost saturated deteriorated state. The fracture network not only completely penetrated the entire sample volume, but also the high-density damaged area further expanded from the center to both ends. The overall distribution of fractures became more uniform. Compared with the sample at 800 °C, the density gradient decreased. This indicates that after crossing the extreme high-temperature critical point, the comprehensive disintegration of the internal structure of the rock will trigger catastrophic consequences. Macroscopically, this is manifested as the spatial convergence of fracture density and the complete loss of overall bearing capacity.

As shown in Figure 6, when heated below 600 °C, the cracks are embryonic. The total thermal cracks in the sample were relatively limited (only 1357). It accumulated slowly as the iterations increased. At this time, the cracks were mainly shear cracks, with a proportion as high as 95 %. This

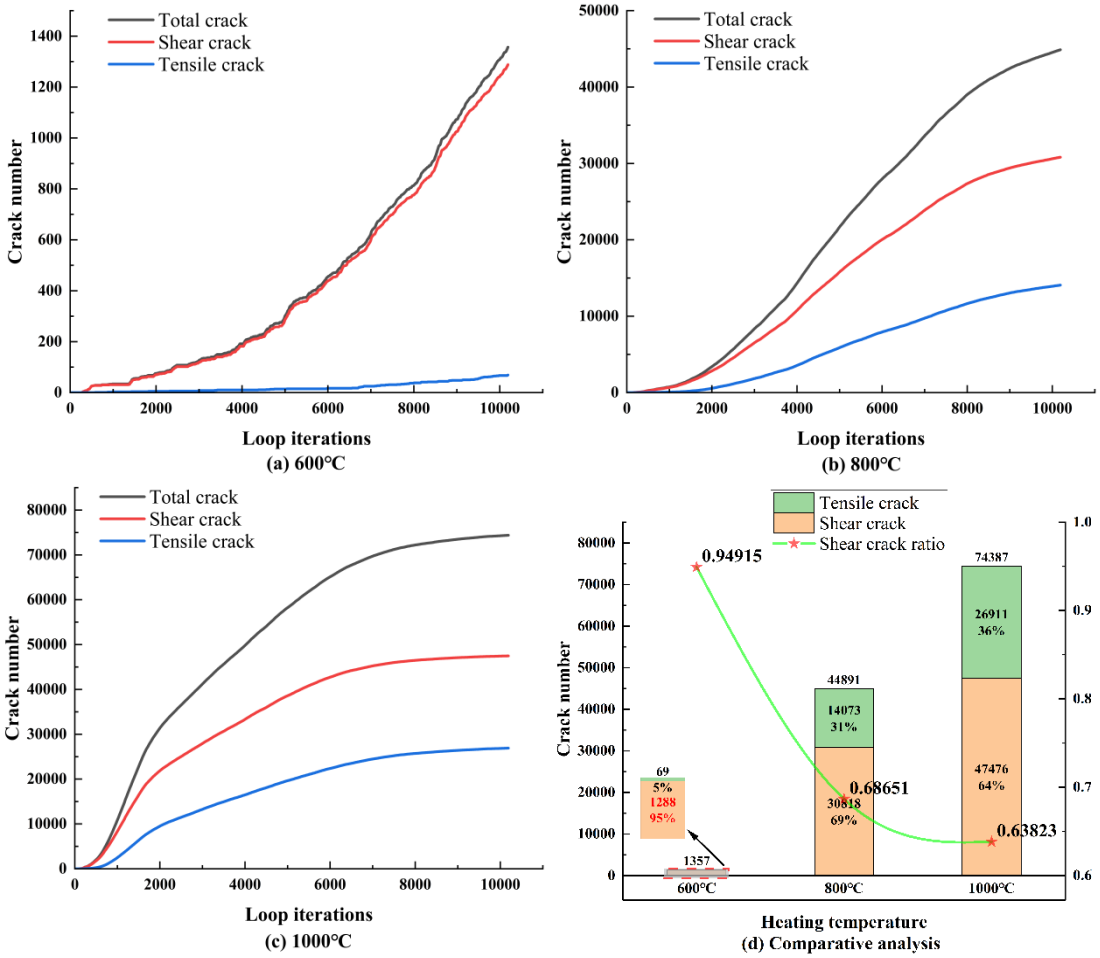

Fig. 6 Relationship and comparative analysis of crack evolution modes and cycle times under different heating temperatures.

phenomenon mainly originated from the base material interface slip caused by the initial local thermal deformation incoordination. However, when the heating temperature increased to 800 ℃ and 1000 ℃, the internal thermal damage evolution entered increased rapidly. The total cracks increased to nearly 45,000 and 74,000 respectively. It showed a significant "early sharp burst, later accelerated convergence" characteristic as the iteration steps increased. More importantly, comparative analysis revealed the characteristic transformation of sandstone high-temperature deterioration: although shear cracks were always the main component of the structure network, the number of tensile cracks caused by extremely high temperatures increased faster. This results in a gradual decrease in the relative proportion of shear cracks, dropping to 69 % and 64 % at 800 ℃ and 1000 ℃, respectively. This evolution pattern conforms to the mechanism of "extremely high non-uniform thermal stress field triggering tensile-shear composite fractures". From a microscopic perspective, the difference between the tensile and shear capabilities of the rock matrix under thermal expansion should be addressed. At extremely high temperatures (800 °C-1000 °C), especially after exceeding the critical temperature threshold, the uneven particle aggregates will undergo intense and asynchronous volume expansion. This uneven thermal expansion will generate a huge normal force at the interface between adjacent particles. Given that the tensile strength of the inter-particle cementation is lower than its shear strength, the expansion stress will rapidly exceed the tensile yield limit. As a result, the adjacent particles will be forcibly torn apart, and tensile micro-cracks will begin to appear before the shear sliding is activated. This indicates that with the continuous increase of temperature, rock damage evolves into a composite mode of large-scale tensile splitting and shear yielding gradually.

3.2. ANALYSIS OF CRACK PROPENSITY DISTRIBUTION AND UNIFORMITY

The spatial distribution characteristics of microcrack tendencies at different temperatures are characterized using rose plots (Fig. 7). When heated to 600 °C, the tensile, shear, and total cracks show certain local preferential orientations. Although tensile cracks are the least, the unevenness of the trend is the most significant, reflecting that the initial thermal stress tends to be concentrated and released along the

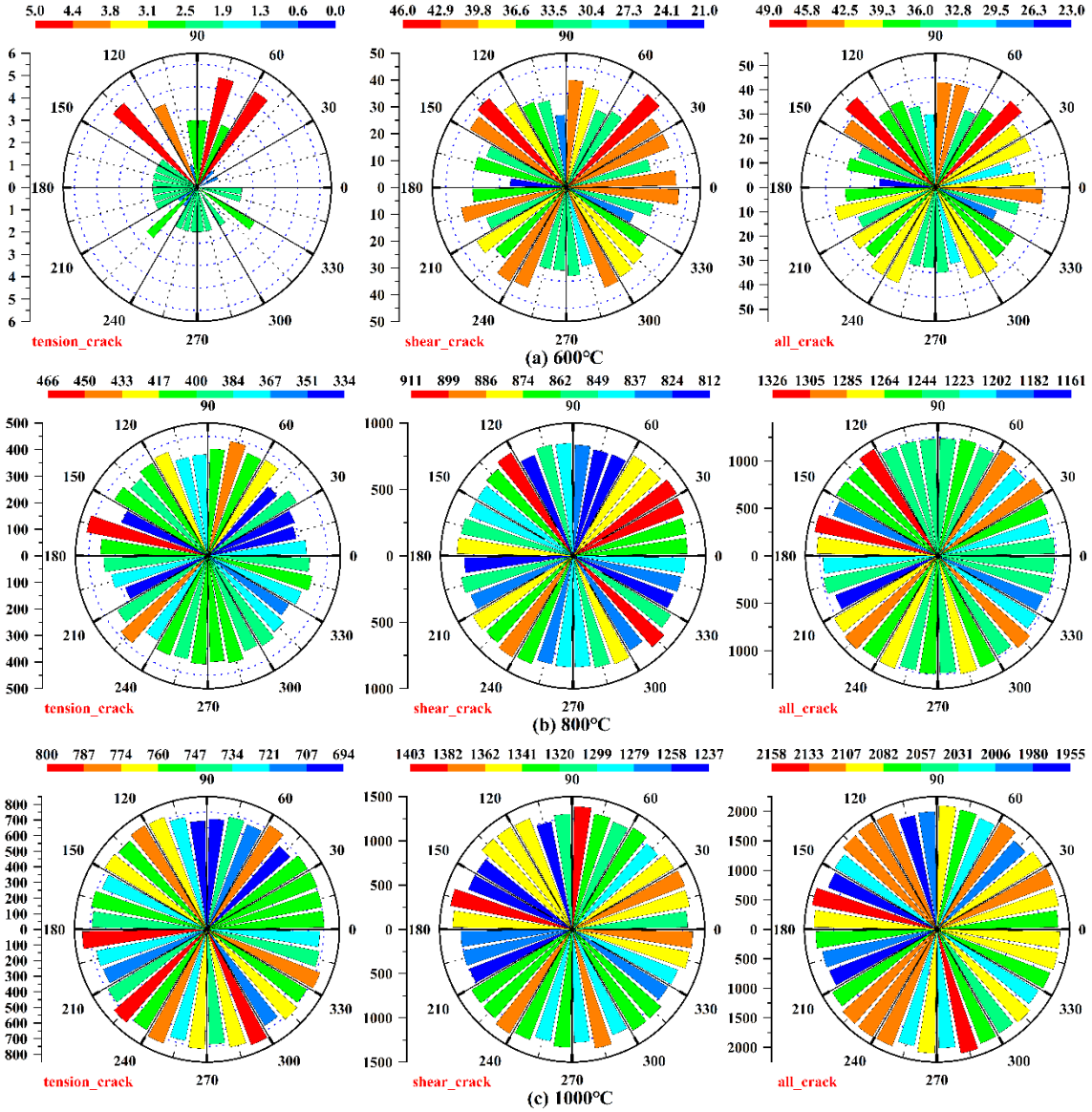

Fig. 7 Increase diagram of crack trend at different temperatures.

original defects or weak bonding points within the rock mass. However, at 800 °C and 1000 °C, the plots of tensile, shear, and total cracks change from the initial non-uniformity to nearly circular equiaxed shapes. This geometric topological feature of the trend towards isotropy reveals the damage mechanism driven by thermal expansion mismatch at high temperatures. They gradually evolve from local directional displacement in the early stage to global disordered random homogeneous disintegration.

To quantitatively characterize the uniformity differences in the distribution of model crack trend, the coefficient of variation (*CV*) and information entropy (*H*) are selected as the two indicators for comparative analysis (Xiong et al., 2023). The coefficient of variation is a statistical indicator representing the dispersion of crack directions in rock masses. Information entropy is used to reflect the disorder or uncertainty of the crack directions in rock masses, defined as follows:

$$CV = \frac{c}{u} \tag{8}$$

$$H = -\sum_{i=1}^{n} p_i \, ln(p_i) \tag{9}$$

where c represents the standard deviation of cracks of different Dip directions; u is the average value of cracks; p_i represents the frequency of cracks (i-th orientation interval), that is, the ratio of cracks in this interval to the total; and n is the total angle grouping intervals.

A lower *CV* indicates that the differences in the number of cracks in different directions are smaller, and the spatial distribution is more uniform. Conversely, it reflects that the development of cracks has a significant directional nature, concentrating mainly in certain advantageous dip directions. Information entropy is not conducive to comparative analysis between different models. Therefore, a normalization is conducted to generate normalized information entropy (Eq. 10), in the range of [0, 1].

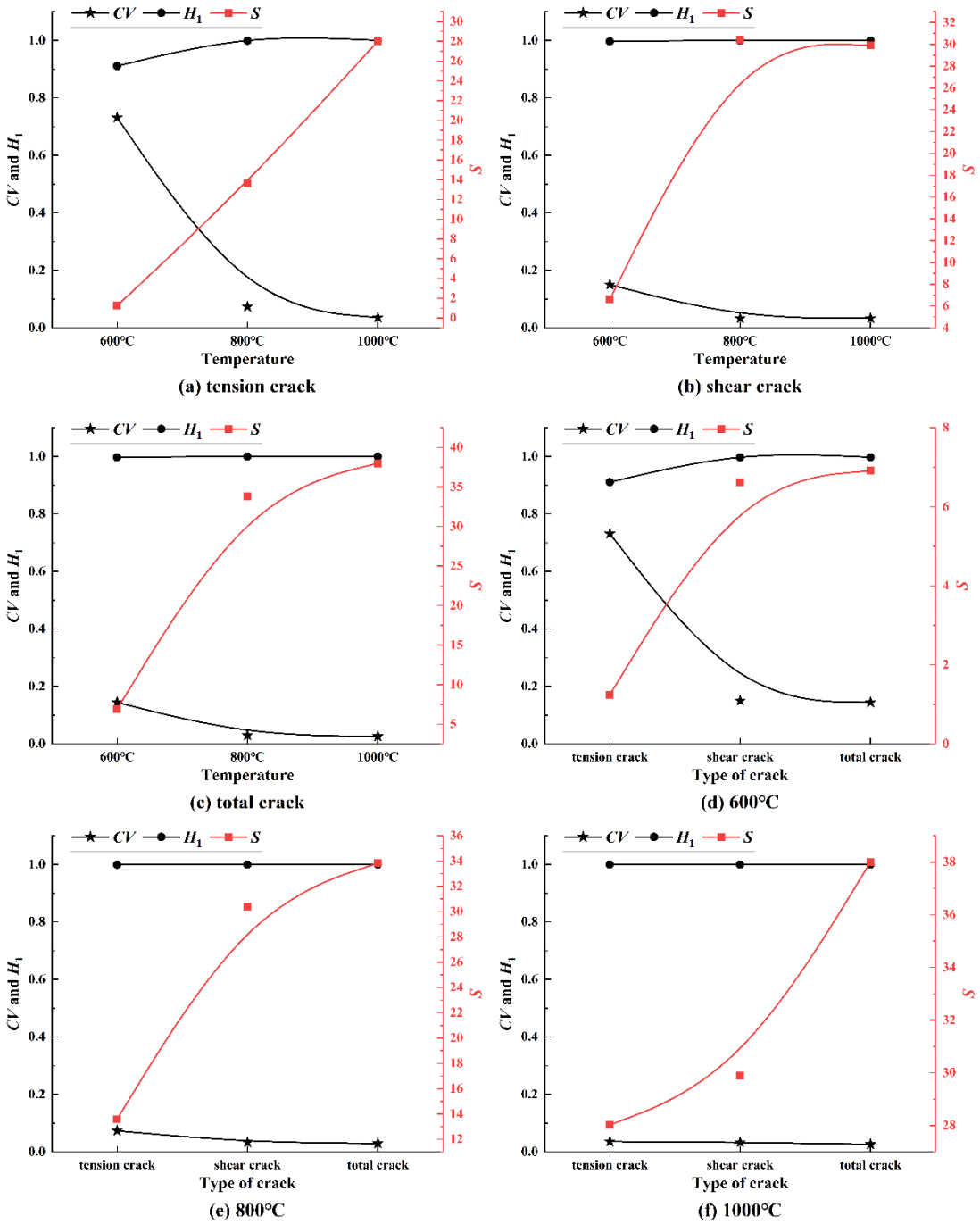

Fig. 8 (a), (b), and (c) show the *CV*, H_1, and *S* values at different heating temperatures within the same crack category; (d), (e), and (f) represent the *CV*, H_1, and *S* values of different crack categories at the same temperature.

When H_1 approaches 1, the dip direction distribution of cracks approaches a completely uniform state.

$$H_1 = \frac{H}{ln(n)} \tag{10}$$

Based on the characterization capabilities of the comprehensive coefficient of variation and information entropy for the anisotropy of fracture distribution, the comprehensive uniformity index *S* is adopted. Combing the two types of statistical parameters, the uniformity of the distribution of dip directions can be evaluated more comprehensively: the larger is *S*, the stronger the uniformity of fracture angle distribution. The expression is as follows:

$$S = \frac{H_1}{CV} \tag{11}$$

The evaluation indicators are affected by the division of the angle range. In this study, the dip direction of the cracks (ranging from 0° to 360°) is evenly divided into n=36 intervals, with an interval spacing of 10° between each interval. Using the Matlab software, a calculation program is written to calculate the coefficient of variation (*CV*), normalized

information entropy (H_1), and the comprehensive uniformity index (S) (Fig. 8).

As shown in Figure 8, as the heating increased from 600 °C to 1000 °C, CV values of tensile cracks, shear cracks, and total cracks all show a significant nonlinear decreasing trend. Meanwhile, H_1 gradually approaches the limit of 1 at a completely uniform state. S values of all types of cracks increase sharply as the temperature increases (Figs. 8(a) to 8(c)). This also indicates that the thermal damage under high-temperature intensifies the disorderly cracking of the microscopic structure in the rock. This causes thermally induced cracks to change from the "directional development" based on local defects to the "isotropic development" without any significant preferred direction. The spatial distribution becomes increasingly uniform. In addition, comparing different cracks laterally (Figs. 8(d) to 8(f)), at lower temperature stages (600 °C), the CV value of tensile cracks have a significantly higher CV value than shear and total cracks. Its S value is at a low point (S<2), indicating that the initial thermally induced tensile cracks have extremely strong direction dependence and local concentration characteristics. However, when the temperature approached 1000 °C, the S values of all types of cracks reached extremely high levels (S>28). The gap between the S values of different cracks is gradually narrowing. Combined with the research on the thermo-mechanical coupling damage of rocks (such as thermal stress-induced cracking and particle interface mismatch mechanism), this phenomenon further confirms that extremely high temperatures are not only an important catalyst for activating shear slip within particles, but also break the anisotropy of crack spatial distributions, promoting the evolution of the overall fracture network towards a uniform and disordered state.

The study examined the characterization of the coefficient of variation, normalized information entropy, and the comprehensive uniformity index. It was found that a single statistical parameter has significant limitations when quantifying thermal damage at high temperatures. As the temperature increases, H_1 rapidly approaches the limit of 1. In the high-temperature range (800-1000 ℃), it has significant saturation and passivation, making it difficult to effectively distinguish the fine evolution of the homogeneity of the fracture network. The CV value can sensitively capture the directional aggregation characteristics of tensile cracks at a relatively low temperature (600 ℃). However, it sharply decays and tends to level off at the extremely high-temperature temperatures. The data range is severely compressed, resulting in a significant decline in resolution under high-temperature thermal damage. In contrast, the indicator S demonstrates excellent evaluation efficiency and sensitivity. Its mathematical construction involves placing the indicator H_1 (approaching 1) in the numerator and the indicator CV (which decays rapidly and approaches 0) in the denominator. Therefore, when high temperature causes random evolution of crack distribution, the S value shows a significant nonlinear amplification. From the amplitude of the graph changes, the S values of various cracks increase from the single-digit range at 600 °C (the lowest point) to the 30-40 range at 1000 °C. This amplification mechanism overcomes the passivation defect of H_1 and the compression effect of CV, presenting hidden uniformity evolution information in the microstructure with higher contrast. This also indicates that the indicator S can track the changes in rock fractures under complex thermal coupling effects more accurately with higher resolution.

3.3. THREE-DIMENSIONAL CONTACT CONFIGURATION

The characterization of contact structure in rock and soil media reveals the arrangement characteristics of the contact sizes and directions between particles in the three-dimensional space. It is a fundamental physical basis to determine the macroscopic mechanical response and strength of the material. Under thermal damage at high temperature, thermal stress will inevitably cause the deterioration of particle contacts, expansion of microcracks, and reconfiguration of force chains, driving significant dynamic changes in the contact structure. Analyzing the contact structure cannot only accurately describe the anisotropy of material thermal damage at high temperature, but also established a mapping relationship between microscopic thermal damage and macroscopic mechanical response.

As shown in Figure 9, from P0 to P600, sandstone undergoes thermal expands, and the intergranular compression leads to non-coordinated accumulation of thermal stress. The contact force structure shows a directional polarization feature. At this stage, the mechanical properties of the sandstone remain optimal. As the temperature increases, the contact force indicated by the color scale continuously increases and peaks at about 600 °C. This indicates that the load-bearing capacity of the system's force chain structure gradually reaches the critical point. However, when heating to 800 °C and 1000 °C, accumulated thermal stress breaks through the cementation strength, triggering an explosive penetration of the network, causing the failure and unloading of the main structure. The three-dimensional structural envelope surface gradually degenerates from the polarized olive shape to a dispersed and sparse elongated form. The magnitude of the contact force decreases. This transition from thermal expansion-induced force chain strengthening to framework collapse triggered by crack coalescence reveals the intrinsic physical mechanism of rock degradation, namely the evolution of rock from an inhomogeneous medium to a low-bearing fragmented structure under extreme high-temperature conditions.

Figure 10 shows the contact number density of different sandstone sample. At the lower heating stages (such as maintaining room temperature, heating

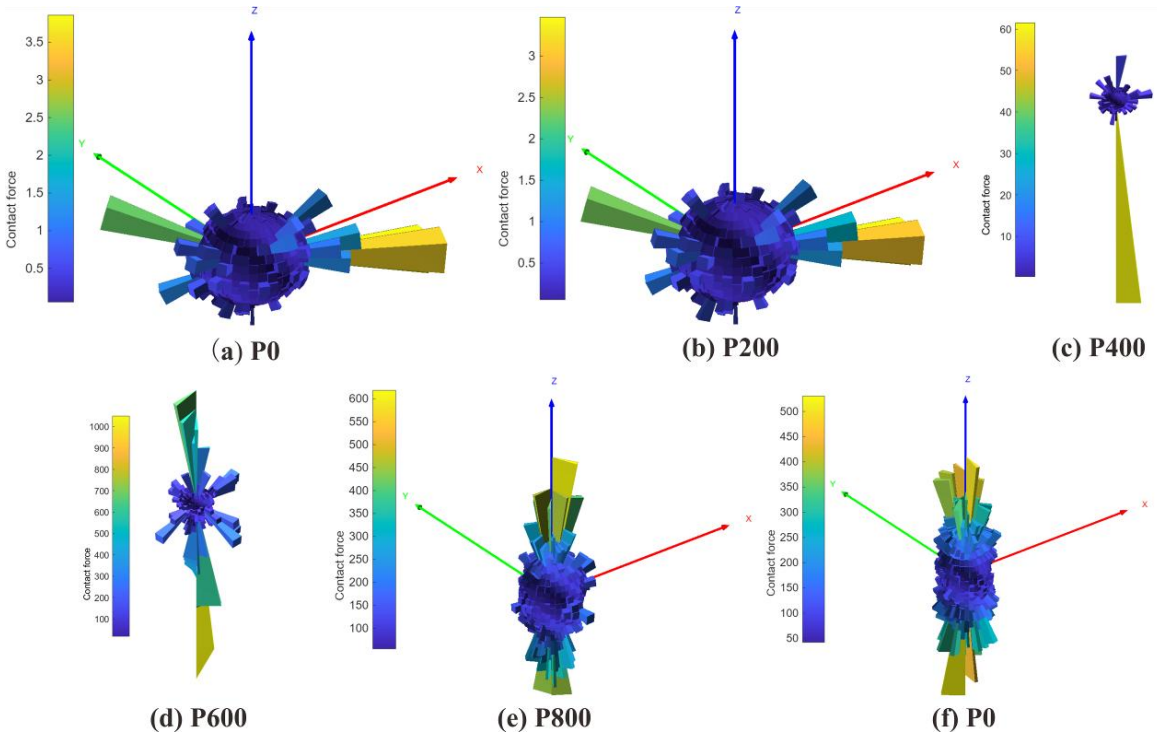

Fig. 9 Three-dimensional structure diagram: contact force of different sandstone samples.

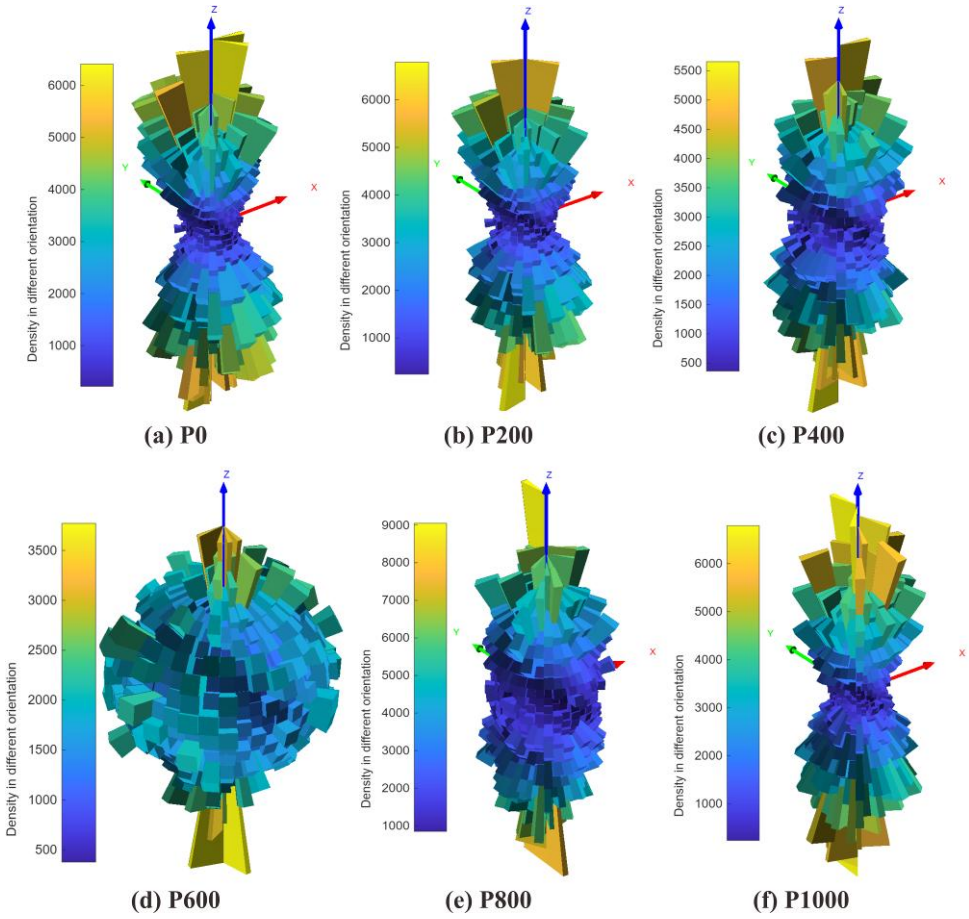

Fig. 10 Three-dimensional structure diagram: contact quantity density of different sandstone samples.

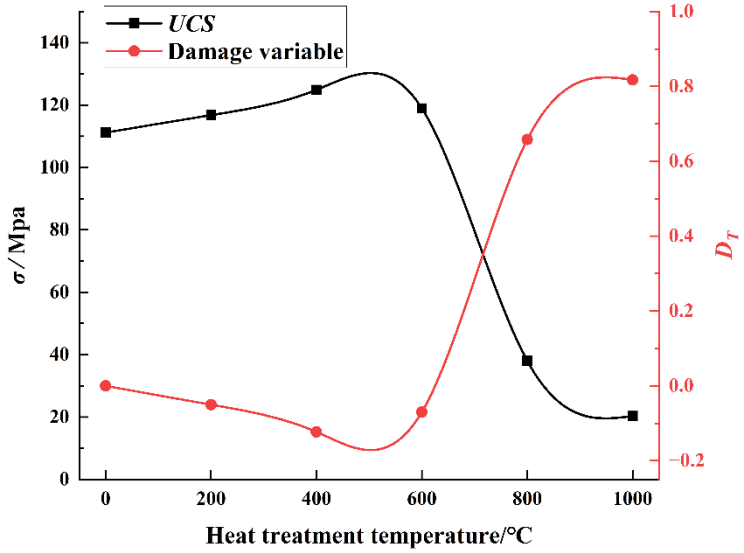

Fig. 11 Uniaxial compressive strength and strength degradation ratio after different heating treatments.

at 200 °C and 400 °C), the contacts are mainly concentrated at the ends of the samples. As the heating temperature gradually increases to 600 °C, the contacts develop from the middle of the sample towards the lateral direction, and the contact density at both ends decreases. This is mainly due to the increase in thermal expansion stress, which enhances the cementation between particles. Therefore, the contact number density map shows a thickening trend. However, as the heating temperature is further increased to 800°C and 1000 °C, the particle bonding is destroyed, resulting in the generation and penetration of large-scale cracks, and a decrease in the contact number. Therefore, the contact number density gradually shrinks and becomes thinner.

3.4. ANALYSIS OF UNIAXIAL COMPRESSIVE STRENGTH AND DAMAGE AT HIGH TEMPERATURES

In rock damage mechanics, macroscopic mechanics are often used to define the damage variable. Given that the uniaxial compressive strength directly explains the integrity of the rock mass skeleton, the strength degradation ratio is adopted to define the thermal damage variable and characterize the failure of the macroscopic bearing skeleton of the rock. The calculation formula is as follows:

$$D_T = 1 - \frac{\sigma_T}{\sigma_0} \tag{12}$$

where D_T represents the thermal damage variable of the rock after being subjected to temperature T treatment, dimensionless; σ_T is the *UCS* of the rock after being treated at high temperature T, MPa; σ_0 is the *UCS* of the rock at normal temperature, MPa. When D_T=0, the rock is intact; when D_T=1, the bearing capacity of the rock his completely disappeared, that is, it is completely broken down.

Figure 11 shows the nonlinear curves of the *UCS* and thermal damage variable (D_T) of sandstone as they change with increasing heating temperature. In the medium-low heating range from 0 °C to about 400 °C (extending to about 600 °C locally), the *UCS* increases mildly and steadily. The thermal damage variable D_T decreases slightly and remains anchored at an extremely low level. This is because as the temperature increases, the particles expand due to heating, making the contact more compact and ultimately increasing compressive strength. However, once the temperature exceeds 600 °C, the *UCS* will decrease sharply, and D_T increases steeply. This is because the intense volume expansion and the mismatch between thermal deformation jointly generate thermal shear stress, inducing explosive crack initiation and propagation, causing the supporting framework to begin to collapse. When the temperature approaches 800 °C to 1000 °C, the *UCS* reaches its minimum value, and the D_T gradually converges to 0.8. The small increase in mechanical properties followed by a sharp decrease reflects the evolution process of the internal contact network of sandstone from a steady state to overall fracture.

To evaluate the effectiveness of this model, the simulation results are compared with the data obtained from the experiments conducted by Bai et al. (2026) (Fig. 12). The simulated *UCS* shows a significant decrease in the range of 600 °C to 800 °C, and the corresponding range obtained from the experiments was between 300 °C and 500 °C. Although the specific temperature points are different, both curves exhibited three highly consistent stages: an initial stable state, a subsequent sharp decline, and finally convergence to a lower residual strength at extremely high temperatures. The consistency of the overall decay pattern confirmed that this model can effectively simulate the mechanical process of sandstone under extreme thermal loads.

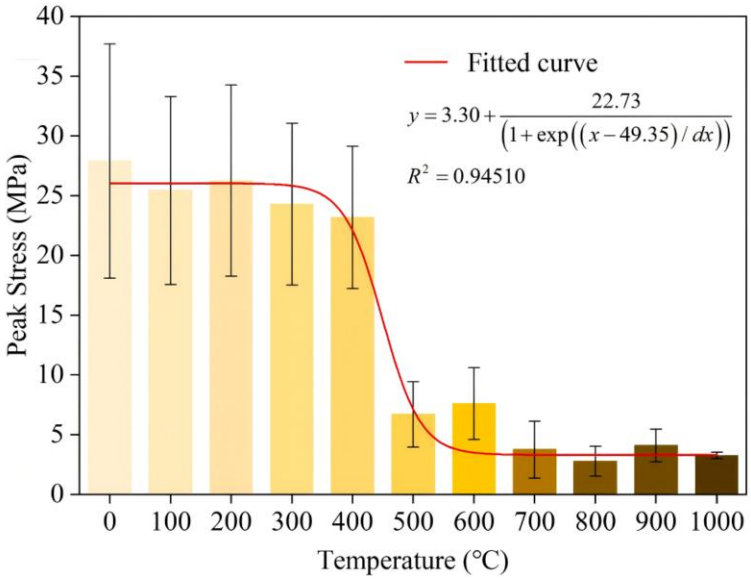

Fig. 12 Experimental validation: Peak stress attenuation curve of sandstone under different high-temperature treatments (Bai et al., 2026).

4. CONCLUSION

The PFC3D simulation technology is used to analyze the thermo-mechanical coupling theory and the three-dimensional uniaxial simulation process. At the same time, it systematically studied the micro-scale damage evolution and mechanism of sandstone a high-temperature. The main results are drawn as follows:

1. The expansion of thermally induced crack has a significant temperature threshold effect and spatial non-uniform characteristic. The critical point for the initiation of internal damage was around 600 ℃. From 800 ℃ to 1000, the cracks grew explosively and penetrated. Due to the asynchronous internal heat conduction and the superposition of thermal stress gradients, the high-density damage zone showed a typical central aggregation effect and decayed to both ends of the sample;
2. High-temperature environment drove the evolution of microcracks. During the incubation period (below 600 °C), the total crack was relatively small. The number of cracks gradually increases with each cycle iteration. Local thermal deformation disorder mainly induces matrix interface slip, and fractures are dominated by shear slip (accounting for 95 %). When gradually increasing to 1000 °C, the total cracks increased sharply. The number of cracks shows a change characteristic of an early rapid outbreak and later accelerated convergence with each cycle iteration. Intense thermal deformation triggered more tensile cracks, and the fracture mode transformed into a combined tensile-shear form;
3. The crack network has undergone an evolution in space from local preferential orientation to overall randomness. The comprehensive uniformity index (S) constructed based on the coefficient of variation and information entropy indicates that at lower temperatures, crack development depends on the original weak surfaces (manifesting strong anisotropy); at extremely high temperatures, the S value nonlinearly increases to a high value. This indicates that the sandstone structure gradually transforms into a disordered isotropic homogeneous disintegration;
4. The three-dimensional contact structure can visually display the spatial distribution and change process of mechanical strength. Below 400 °C, the thermal expansion and compaction effect caused the internal force chains to polarize and became locally strengthened. This resulted in a slight increase in the uniaxial compressive strength (UCS), and the thermal damage variable slightly decreased and approached an extremely low value. Once it exceeds 600 °C, the contact structure diagram changes from the polarized olive shape to a sparse and dispersed elongated form. The main force transmission framework collapses, causing the UCS to drop rapidly, and the thermal damage variable approaches 0.8.

This study systematically investigates the threshold effect of high-temperature thermal damage in sandstone, the evolutionary characteristics of thermal cracks, and the mesoscopic mechanism of force chain skeleton collapse. The findings can provide a theoretical basis for predicting rock mass instability in deep underground engineering, and practical guidance for the support design of deep high-temperature surrounding rock as well as the prevention and mitigation of geothermal disasters. However, deep reservoirs are often in a complex environment of heat, seepage, stress, and chemistry, and are subject to dynamic disturbances (such as mechanical rock breaking or seismic waves). Future research will incorporate seepage and chemical fields

to reveal the rock failure mechanism under multi-field coupling conditions, and further explore the fatigue damage behavior of high-temperature rock masses subjected to dynamic loading.

ACKNOWLEDGMENTS

This work was supported by the National Key R&D Program of China [grant number 2011CB013501], National Natural Science Foundation of China [grant number 41272333], the Sichuan Transportation technology project [grant number 2021-ZL-03].

DATA AND CODE AVAILABILITY

All data generated or used during the study is available from the corresponding author upon reasonable request.

COMPETING INTERESTS

The authors declared that there was no conflict of interest here.

REFERENCES

Alneasan, M., Alzo'ubi, A.K. and Ibrahim, F.: 2024, A comparison between conventional and generalized fracture criteria to predict fracture parameters in clay rich rocks (Mudstone) under temperature effect. Constr. Build. Mater., 416, 135168. DOI: 10.1016/j.conbuildmat.2024.135168

Bai, J.W., Da, G., Li, J., Feng, G.R. and Wang, Z.: 2026, Effects of high temperature on the energy-based brittle-ductile transition characteristics and mechanism of coal specimens. Fuel, 415, 138426. DOI: 10.1016/j.fuel.2026.138426

Bao, X.K., Huang, S.J., Lv, Y.J., Huang, Y., Wang, L.Z. and Zhang, X.F.: 2025, Study on Kaiser effect of granite under cyclic loading and unloading at different temperatures. Sci. Rep., 15, 1, 11898. DOI: 10.1038/s41598-025-90733-6

Chen, Z.Q., He, C., Ma, G.Y., Xu, G.W. and Ma, C.C.: 2019, Energy damage evolution mechanism of rock and its application to brittleness evaluation. Rock Mech. Rock Eng., 52, 4, 1265–1274. DOI: 10.1007/s00603-018-1681-0

Dang, Y.K., Yang, Z., Yang, S.T. and Liu, X.Y.: 2025, Thermal damage and crack propagation mechanisms of defective crystalline rocks: An experimental and numerical investigation. Theor. Appl. Fract. Mech., 139(Part B), 105113. DOI: 10.1016/j.tafmec.2025.105113

Feng, W.L., Qiao, C.S., Wang, T., Yu, M.Y., Niu, S.J. and Jia, Z.Q.: 2020, Strain-softening composite damage model of rock under thermal environment. Bull. Eng. Geol. Environ., 79, 8, 4321. DOI: 10.1007/s10064-020-01808-9

Garrido, M.E., Petnga, F.B., Martínez-Ibáñez, V., Serón, J.B., Hidalgo-Signes, C. and Tomás, R.: 2022, Predicting the uniaxial compressive strength of a limestone exposed to high temperatures by Point Load and Leeb Rebound Hardness Testing. Rock Mech. Rock Eng., 55, 1, 1–17. DOI: 10.1007/s00603-021-02647-0

Griffiths, L., Heap, M.J., Lengliné, O., Baud, P., Schmittbuhl, J. and Gilg, H.A.: 2024, Thermal stressing of volcanic rock: Microcracking and crack closure monitored through acoustic emission, ultrasonic velocity, and thermal expansion. J. Geophys. Res., Solid Earth, 129, 3, e2023JB027766. DOI: 10.1029/2023JB027766

Günindi, B., Toygar, M.E. and Tümer, D.: 2024, Design and heat analysis of basalt glass as a thermal storage material in a concentrated solar power (CSP) system. J. Therm. Anal. Calorim., 149, 5, 2007–2023. DOI: 10.1007/s10973-023-12815-9

Guo, Y.D., Li, X.B. and Huang, L.Q.: 2023, Experimental investigation on the sudden cooling effect of oil-based drilling fluid on the dynamic compressive behavior of deep shale reservoirs. Energy, 282, 128680. DOI: 10.1016/j.energy.2023.128680

Harshini, R.D.G.F., Ranjith, P.G. and Kumari, W.G.P.: 2024, Australia's geothermal frontier: Unlocking Granite's energy secrets. Geoenergy Sci. Eng., 234, 212665. DOI: 10.1016/j.geoen.2024.212665

Hu, X.J., Qi, Y.J., Hu, H.B., Lei, G., Xie, N. and Gong, X.A.: 2023, A micromechanical-based failure criterion for rocks after high-temperature treatment. Eng. Fract. Mech., 284, 109275. DOI: 10.1016/j.engfracmech.2023.109275

Huang, H., Meakin, P. and Malthe-Sorenssen, A.: 2016, Physics-based simulation of multiple interacting crack growth in brittle rocks driven by thermal cooling. Int. J. Numer. Anal. Methods Geomech., 40, 16, 2163–2177. DOI: 10.1002/nag.2523

Liu, X.C., Huang, F., Zheng, A.C. and Yang, D.: 2025, Effects of two different cooling impact treatments on the thermal damage and mechanical properties of high-temperature granite. Case Stud. Therm. Eng., 66, 105716. DOI: 10.1016/j.csite.2024.105716

Pham, M.T., Weng, M.C., Le, H.K., Lin, S.S. and Wu, W.H.: 2024, Evaluating the anisotropic thermal-mechanical coupling strength of slate: A discrete element method approach. Comput. Geotech., 171, 106368. DOI: 10.1016/j.compgeo.2024.106368

Potyondy, D.O.: 2015, The bonded-particle model as a tool for rock mechanics research and application: current trends and future directions. Geosystem Eng., 18, 1, 1–28. DOI: 10.1080/12269328.2014.998346

Ram, B.K., Das, R. and Mishra, D.A.: 2025, Thermal treatment induced damage mechanism of rock materials and its influence on the physico-mechanical properties-a review. Environ. Earth Sci., 84, 12, 334. DOI: 10.1007/s12665-025-12300-6

Ranjith, P.G., Zhao, J., Ju, M.H., De Silva, R.V.S., Rathnaweera, T.D. and Bandara, A.K.M.S.: 2017, Opportunities and challenges in deep mining: A brief review. Engineering, 3, 4, 546-551. DOI: 10.1016/J.ENG.2017.04.024

Rezaee, H. and Noorian-Bidgoli, M.: 2025, Numerical and experimental investigations of grain size and temperature effects on the crack propagation velocity in brittle rocks. Comput. Part. Mech., 12, 5, 2969–2981. DOI: 10.1007/s40571-025-00962-9

Sharafisafa, M., Aliabadian, Z., Sato, A. and Shen, L.M.: 2023, Coupled thermo-hydro-mechanical simulation of hydraulic fracturing in deep reservoirs using Finite-Discrete Element Method. Rock Mech. Rock Eng., 56, 7, 5039–5075. DOI: 10.1007/s00603-023-03325-z

Showkati, A., Salari-rad, H. and Aghchai, M.H.: 2021, Predicting long-term stability of tunnels considering rock mass weathering and deterioration of primary support. Tunn. Undergr. Space Technol., 107, 103670. DOI: 10.1016/j.tust.2020.103670

Sun, B.W., Yang, S.Q., Li, H. and Tian, W.L.: 2024, Multiscale study of dynamic mode-I fracture characteristics of thermally treated granite: Comparison of conventional and microwave heating. Eng. Fract. Mech., 310, 110478. DOI: 10.1016/j.engfracmech.2024.110478

Tomás, R., Benavente, D., Martínez-Ibáñez, V. and Garrido, M.E.: 2025, How do high temperatures affect rock properties? A comprehensive review of experimental thermal effects and underlying mechanisms. Eng. Geol. 357, 108323. DOI: 10.1016/j.enggeo.2025.108323

Vidana Pathiranagei, S. and Gratchev, I.: 2021, Engineering properties of sandstone heated to a range of high temperatures. Bull. Eng. Geol. Environ., 80, 3, 2415–2432. DOI: 10.1007/s10064-020-02065-6

Wang, Q.Y., Wang, D.B., Yu, B., Sun, D.L., Wang, Y.L., Hao, N. and Han, D.X.: 2024, Evolution of elastic-plastic characteristics of rocks within middle-deep geothermal reservoirs under high temperature. Nat. Resour. Res., 33, 4, 1573–1596. DOI: 10.1007/s11053-024-10342-4

Wanne, T.S., and Young, R.P.: 2008, Bonded-particle modeling of thermally fractured granite. Int. J. Rock Mech. Min. Sci., 45, 5, 789–799. DOI: 10.1016/j.ijrmms.2007.09.004

Wu, S.S., Ma, X.X., Zhang, X.H., Chen, J.H., Yao, Y. and Li, D.Q.: 2024, Investigation into hydrogen induced fracture of cable bolts under deep stress corrosion coupling conditions. Tunn. Undergr. Space Technol., 147, 105729. DOI: 10.1016/j.tust.2024.105729

Wu, X.G., Huang, Z.W., Cheng, Z., Zhang, S.K., Song, H.Y. and Zhao, X.: 2019, Effects of cyclic heating and LN2-cooling on the physical and mechanical properties of granite. Appl. Therm. Eng., 156, 99–110. DOI: 10.1016/j.applthermaleng.2019.04.046

Xiong, W., Chen, Y.X. and Ma, S.G.: 2023, Unified model-free interaction screening via CV-entropy filter. Comput. Stat. Data Anal., 180, 107684. DOI: 10.1016/j.csda.2022.107684

Yin, H., Huang, Y.H., Zhang, K.B., Liu, X.W., Peng, J. and Li, M.X.: 2025, Fracture characteristics of granite specimens after heating-cooling treatments: Insights from experiments and GBM simulations. Comput. Geotech., 182, 107160. DOI: 10.1016/j.compgeo.2025.107160

Yin, T.B., Men, J., Lu, J.F., Wu, Y., Guo, W.X., Yang, Z. and Ma, J.X.: 2024, Study on dynamic mechanical properties and microscopic damage mechanisms of granite after dynamic triaxial compression and thermal treatment. Case Stud. Therm. Eng., 61, 104910. DOI: 10.1016/j.csite.2024.104910

Yoo, H., Yoon, J. and Min, K.B.: 2023, Effect of rock mass properties on coupled thermo-hydro-mechanical responses at near-field rock mass in a heater Test-A Benchmark Sensitivity study of the Kamaishi Mine experiment in Japan. J. Nucl. Fuel Cycle Waste Technol., 21, 1, 23–41. DOI: 10.7733/jnfcwt.2023.007

Zhu, X.H., Wang, Y.F. and Liu, W.J.: 2025, Investigation of rock-cutting behaviour in high-temperature and high-pressure conditions. Proc. Inst. Civ.: Geotech. Eng., 178, 7, 842–859. DOI: 10.1680/jgeen.25.00034